Fluid Phase Equilibria 495 (2019) 28–32

Contents lists available at ScienceDirect

Fluid Phase Equilibria

journal homepage: www.elsevier.com/locate/fluid

Determination of pressure-viscosity relation of 2,2,4-trimethylhexane by all-atom molecular dynamics simulations

Marco A. Galvani Cunha, Mark O. Robbins*

Department of Physics & Astronomy, Johns Hopkins University, Baltimore, MD, 21218, United States

ARTICLE INFO

Article history:
Received 6 February 2019
Received in revised form
9 May 2019
Accepted 10 May 2019
Available online 16 May 2019

Keywords:
2,2,4-trimethylhexane
Pressure-viscosity
AIREBO-M
Elastohydrodynamic
Lubrication

ABSTRACT

The Newtonian viscosity of 2,2,4-trimethylhexane at 293 K is determined at pressures from 0.1 MPa to 1000 MPa. Non-equilibrium molecular dynamics simulations are performed using AIREBO-M, an all-atom potential for hydrocarbons especially parameterized for high pressures. The steady-state shear stress and viscosity are determined from simple shear simulations at rates between 10^7 and $5{\cdot}10^9$ s^{-1}. At low pressures, simulation rates are low enough to reach the Newtonian regime. At high pressures, results are extrapolated to the Newtonian limit by fitting rate-dependent viscosities to Eyring theory. The variation of viscosity with pressure has an inflection point that is common for small molecules. Deviations from experiment are less than 40%.

1. Introduction

The 10th Industrial Fluid Properties Simulation Challenge tasked simulators with predicting the pressure dependence of the Newtonian viscosity η_N of a simple hydrocarbon liquid using any molecular modeling method. The hydrocarbon chosen was 2,2,4-trimethylhexane (Fig. 1), and its viscosities were measured at pressures of 0.1, 25, 50, 100, 150, 250, 400, 500, 600, 700, 800, 900 and 1000 MPa. Here we present calculations of the viscosities at these pressures using all-atom nonequilibrium molecular dynamics simulations. This paper was originally submitted as an entry to the challenge and won. After the release of the results we added the benchmark data to our plot of the pressure-viscosity relation, Fig. 3, and added a discussion of the comparison between the results to the discussion.

This challenge was timely because the pressure dependence of fluid viscosities plays a critical role in elastohydrodynamic lubrication (EHL) [1–3] and faster computers are enabling calculation of fluid response at strain rates ($\sim 10^5$ s^{-1}) approaching experiments for the first time [4,5]. In addition there has been an active debate about the connection between molecular-scale processes and the rate and pressure dependence of viscosity [6–8].

Non-equilibrium molecular dynamics simulations have long been used to determine thermal and transport properties of simple hydrocarbons [9]. Many of the early papers focused on the temperature dependence of viscosity [10–13], including measures important to lubricant function [12,13]. Some early studies of the high pressures typical of EHL conditions considered molecules in strongly confined geometries where layering and interfacial interactions alter the viscosity [14,15]. Later, trends with pressure were studied using periodic boundary conditions to eliminate interfacial effects [16–19]. Several simple hydrocarbons were studied using united-atom potentials at state points where molecular relaxation times were short enough that the Newtonian regime could be reached at the high shear rates (10^9 to $2{\cdot}10^{11}$ s^{-1}) accessible to computers at that time. These simulations found that united-atom potentials generally under-predicted the viscosity but reproduced experimental trends with temperature, pressure, rate and molecular structure [16–19].

At pressures typical of EHL conditions, molecular relaxation times often become too long for direct evaluation of the viscosity even with current computers. Here we follow the recent study of squalane by Jadhao and Robbins [5]. Nonequilibrium molecular dynamics simulations of simple shear are performed as a function of strain rate $\dot{\gamma}$ at each pressure p. At low pressures, simulation rates are low enough to reach the Newtonian regime, and η_N is evaluated directly from the calculated limiting viscosity. As p and η_N rise, relaxation times become longer than our simulation times, and we

* Corresponding author.
E-mail address: mr@jhu.edu (M.O. Robbins).

https://doi.org/10.1016/j.fluid.2019.05.008
0378-3812/

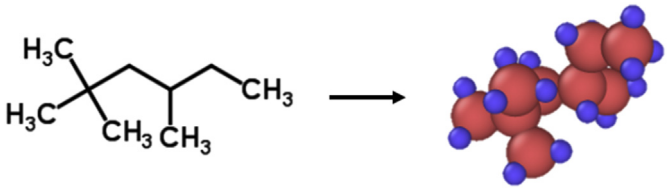

Fig. 1. 2,2,4-trimethylhexane molecule and its representation in our all-atom simulations. Carbons are shown as large red spheres and hydrogens as small blue spheres. The sphere sizes are not representative of the interaction potential.

can not reach the Newtonian regime. Values of η_N for these high pressures are obtained by fitting the rate-dependent shear stress to the Eyring model [20].

2. Methods

A key factor in the accuracy of calculated viscosities is the choice of interaction potential [9,21]. As noted above, past united-atom simulations have tended to underestimate the viscosity of hydrocarbons [12,16,19]. Our past work showed that united-atom and all-atom potentials gave similar results for the large molecule squalane [5], but an all-atom potential was required for the small molecule cyclohexane. We thus chose to use an all-atom potential for simulations of 2,2,4-trimethylhexane whose geometry is shown in Fig. 1.

One common all-atom potential is the Adaptive Intermolecular Reactive Empirical Bond Order (AIREBO) potential [22], which uses the reactive bond order (REBO) potential [23] for intramolecular energies and a Lennard-Jones (LJ) potential for intermolecular interactions. It has been used successfully in many simulations of hydrocarbons at ambient pressure but over-predicts the stiffness of alkanes at high pressures due to the strong divergence in the LJ potential. O'Connor et al. [24] developed a modified version of AIREBO called AIREBO-M that substitutes the LJ intermolecular interaction with a Morse potential. This softens the repulsive region, leading to better agreement with experimental data at high pressures. The potential was parameterized using x-ray data for the C—C separation in graphite and high-quality quantum chemistry calculations for C—H and H—H interactions. It was then validated against shock Hugoniot and crystal structure data for polyethylene at pressures up to 40 GPa.

We determined the Newtonian viscosity of 2,2,4-trimethylhexane using non-equilibrium molecular dynamics (NEMD) simulations with AIREBO-M and the protocol used by Jadhao and Robbins to determine the viscosity of squalane [5]. All simulations were performed with the molecular dynamics package LAMMPS using standard protocols [25]. The simulations were initialized by placing 1000 randomly oriented molecules of 2,2,4-trimethylhexane far apart from each other in a simulation box with periodic boundary conditions. The box was then compressed slowly to reach the experimental density at room temperature and pressure and this initial state was equilibrated at a temperature of 293 K for 2.5 ns using a Nosé-Hoover thermostat. The system was then brought to the desired pressure and equilibrated over 5ns using a Nosé-Hoover barostat. Different protocols for equilibration and changes in pressure and temperature gave equivalent results within statistical error bars. The timestep used for results below was 0.5 fs, and the thermostat and barostat time constants were 0.5 ps and 5.0 ps, respectively. Both time constants are longer than the relevant correlation times in the system.

Simple shear simulations were done at constant density using standard NEMD methods. We imposed a shear velocity profile by deforming the periodic simulation cell at a constant strain rate and integrating the SLLOD equations of motion [26]. We determined the shear stress σ by calculating the off-diagonal component of the stress tensor during the run, and monitored relevant state variables (temperature, pressure and shear stress) to determine when the system reached steady-state. Strains of order 10 were used to gather enough independent samples in steady-state for most pressures and strain rates. Only rates up to 5×10^9 s^{-1} were considered because heating and other nonequilibrium effects were noticeable for squalane at 10^{10} s^{-1} [5] and the goal of the challenge was to determine the low rate viscous response.

During each simulation we acquired values for the components of the stress tensor averaged over successive time intervals of 5 ps. After reaching steady-state, these data were averaged to obtain the mean shear stress and pressure. Since correlation times change with pressure and strain rate, care is needed in determining the statistical uncertainty in the average. For each run, a block time-averaging method is used [27]. The variance of the distribution of block averages is calculated as a function of block size. Initially the variance rises with block size since sequential samples are correlated, but after the block size exceeds the correlation time the variance saturates to the true error on the mean. For the one run at the lowest rate, 10^7 s^{-1}, the simulation ran for a strain less than unity and may not have reached steady state. This introduces an additional systematic uncertainty that was estimated as about twice the uncertainty from block averages by looking at data from higher rates.

All runs are done at fixed density and the corresponding pressure may differ slightly from that set in the equilibration run, particularly at high pressures where the relaxation times are long. The pressure for the chosen density was determined by extrapolating $p(\dot{\gamma})$ to zero strain rate. In the Newtonian regime, the diagonal components of the stress tensor change quadratically with rate and shear stress. Recent studies indicate this quadratic dependence on σ extends into the non-Newtonian regime [28] and quadratic fits for each density were used to extrapolate the pressure to zero strain rate. Improved statistics after the deadline for the challenge led to shifts that are consistent with the initial error bars and were largest for $p \geq 800$ MPa ($\sim$ 1 to 2%).

At the highest pressures, the response remains non-Newtonian at the lowest accessible strain-rates. Following Ref. [5], we obtained a value for the Newtonian viscosity by fitting high rate results to Eyring theory. The Eyring model assumes that flow occurs via thermally activated hops over an energy barrier that decreases linearly with the applied shear stress σ. Combining the probabilities of forward and backward hops leads to the Eyring equation relating strain rate and stress:

$$\dot{\gamma} = \frac{\sigma_E}{\eta_N} \sinh(\sigma/\sigma_E) \ , \tag{1}$$

where the Eyring stress σ_E is related to the sensitivity of the energy barrier to shear stress. At large stresses $\sigma \sim \log\dot{\gamma}$ and both parameters in the Eyring model, η_N and σ_E, can be obtained from a simple straight-line fit to a linear-log plot.

3. Results

Fig. 2 shows results for the shear stress σ and nonequilibrium viscosity $\eta(\dot{\gamma}) = \sigma/\dot{\gamma}$ as a function of shear rate for each pressure. The points at strain rates of $3 \cdot 10^7$ s^{-1} and $2.5 \cdot 10^9$ s^{-1} were obtained after the submission to the challenge. We include them in our analysis below but the resulting changes in η_N are less than the errorbars in our original submission.

At pressures less than 250 MPa there is no statistically

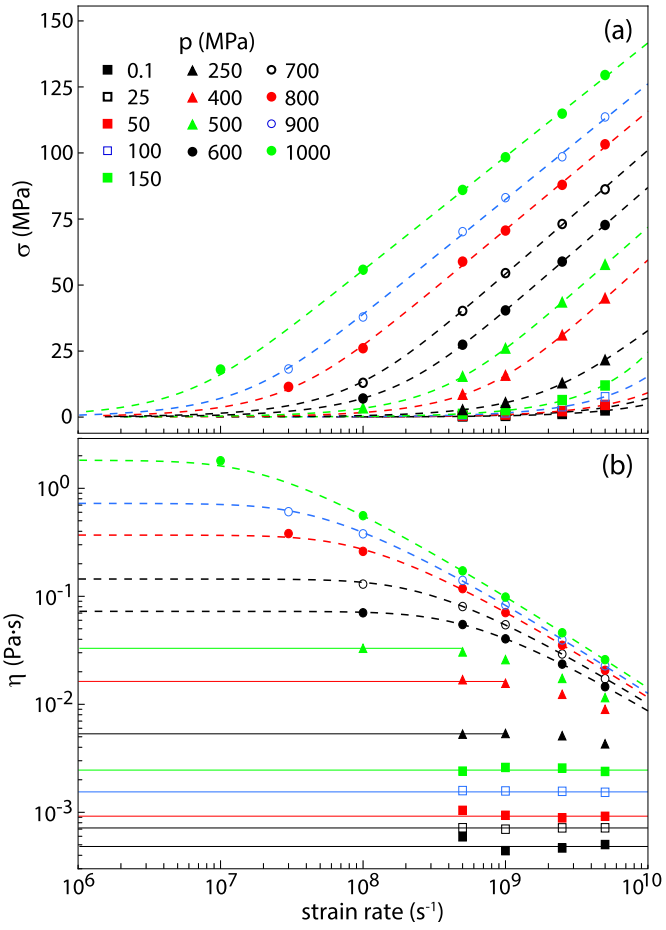

Fig. 2. (a) Stress and (b) viscosity as a function of strain rate at $T = 293$ K and the indicated pressures. Higher curves are for higher pressures in each panel. Symbol types are used to indicate how η_N was obtained. Squares indicate that all data were in the Newtonian regime and the reported η_N is a weighted average over all data. Triangles indicate pressures where the lowest two rates had reached the Newtonian limit and were averaged to determine η_N. Horizontal solid lines in panel (b) indicate the average viscosity obtained for these pressures (squares and triangles). Eyring fits (dotted lines) were used to determine η_N for the higher pressures indicated by circles. These fits are shown for $p \geq 600$ MPa in panel (b) and for all pressures in panel (a), where they should only be considered guides to the eye for $p \leq 500$ MPa. Data at strain rates of $3 \cdot 10^7$ s^{-1} and $2.5 \cdot 10^9$ s^{-1} were obtained after the contest submission. Statistical error bars are only larger than the symbol size for $p = 0.1$ and 25 MPa at the lowest rate shown where they are about twice the symbol size.

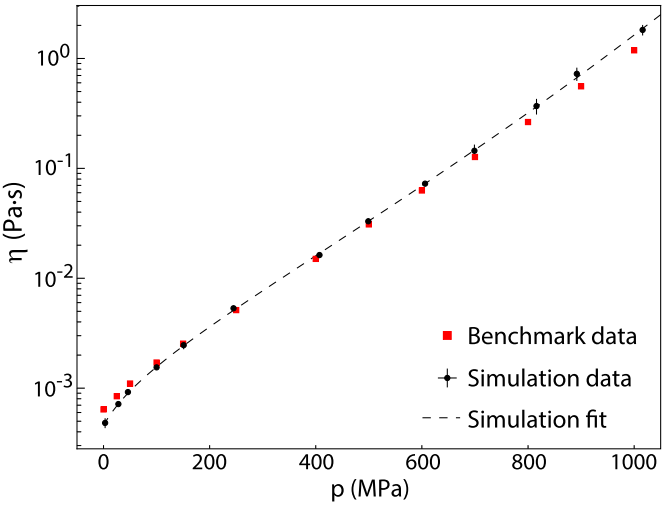

Fig. 3. Pressure-viscosity relation for 2,2,4-trimethylhexane. Simulation data is from Table 1, and statistical error bars are shown when larger than the symbol size. The dashed line is a fit to Eq. (2) with coefficients $\eta_0 = 0.46 \pm 0.02$ mPa·s, $C_F = 27 \pm 9$, $p_\infty = 5.2 \pm 1.2$ GPa, $a_0 = 0.015 \pm 0.004$ MPa^{-1}, $q = 0.5 \pm 0.2$.

Table 1
Nonequilibrium simulations were done as a function of rate at the indicated densities ρ. Values for the corresponding pressure and viscosity in the Newtonian limit were obtained as described in Methods.

ρ (kg/m3)	p(MPa)	η_N(mPa·s)
710	3.0 ± 0.2	0.48 ± 0.05
742	28 ± 1	0.72 ± 0.03
758	46 ± 1	0.92 ± 0.05
791	100 ± 1	1.55 ± 0.04
814	151 ± 1	2.5 ± 0.2
846	245 ± 1	5.3 ± 0.3
885	407 ± 3	16.2 ± 1
903	499 ± 2	33 ± 2
921	606 ± 2	73 ± 3
935	699 ± 2	144 ± 20
950	816 ± 3	370 ± 60
960	892 ± 4	720 ± 100
974	1016 ± 4	1820 ± 200

significant rate dependence in $\eta(\dot{\gamma})$ at the rates studied, indicating that relaxation times are less than 0.1 ns. As p increases, shear thinning becomes more pronounced, and sets in at progressively lower rates. For $p \leq 500$ MPa the lowest simulation rates appear to reach a plateau corresponding to the Newtonian viscosity. At higher pressure, η increases significantly between the lowest two shear rates.

Values of η_N were obtained from the above simulation data following the procedure of Ref. [5]. For $p \leq 500$ MPa the Newtonian viscosity in Table 1 was obtained from an average over points in the plateau weighted by the statistical uncertainty obtained as described in the previous section. Squares in Fig. 2 indicate pressures where all rates were used in the average. Triangles indicate pressures where the lowest two rates were averaged. Horizontal solid lines in Fig. 2 (b) show the Newtonian viscosity obtained from these averages.

The dashed lines at higher pressures in Fig. 2(b) and at all pressures in Fig. 2(a) are fits to Eyring theory. For $p \leq 500$ MPa they should be considered as guides to the eye because the range of shear thinning is not sufficient to distinguish between different models of shear thinning and earlier work has shown that Eyring theory only applies at high pressures [5,28].

Eyring theory provides a good fit to data for 2,2,4-trimethylhexane at $p \geq 600$ Mpa. The slope in plots of σ against the logarithm of strain rate is proportional to the Eyring stress σ_E. As for squalane [5], σ_E is nearly independent of pressure at fixed temperature and the fits for $p \geq 600$ MPa all give $\sigma_E = 20 \pm 1$ MPa. In Eyring theory, $\sigma_E = k_B T / V^*$, where V^* is called the activation volume and represents the sensitivity of the energy barrier to stress. While V^* need not correspond to any actual volume, fits frequently give values comparable to the molecular volume. The fits in Fig. 2 correspond to $V^* \approx 0.2$ nm^3 which is close to the molecular volume of 0.29 nm^3.

Eyring fits were used to determine the values of η_N in Table 1 for $p \geq 600$ MPa. Because this represents an extrapolation, the error in η_N is more difficult to estimate. The quoted errors are the larger of the uncertainty in η at the lowest $\dot{\gamma}$ and the calculated uncertainty in the fit. The ratio of the extrapolated η_N to the largest calculated value was up to a factor of 1.7 for $p = 800$ and 900 MPa using the data available at the time of submission. Adding data at $3 \cdot 10^7$ s^{-1} reduced the need for extrapolation and yielded the same value of η_N within statistical errors.

Fig. 3 shows the Newtonian viscosity as a function of pressure from Table 1. Note that there is an inflection point in the data at a pressure of around 500–600 MPa. This type of curve is commonly observed in experimental plots of $\log\eta_N$ against pressure and procedures have been developed for fitting it.

Paluch [29] proposed a pressure-viscosity relation that assumes the existence of a finite pressure p_∞ at which relaxation times diverge at a given temperature. It is analogous to the temperature where η_N diverges in a Vogel-Fulcher-Tammann (VFT) [30–32] theory for the glass transition. McEwen [33] proposed a relation that explained the slower than exponential rise with pressure seen at low p. Bair [34] combined the Paluch and McEwen equations into a single relation called the hybrid model:

$$\eta = \eta_0 \exp\left(\frac{C_F p}{p_\infty - p}\right)(1 + a_0 p/q)^q \quad (2)$$

The dotted line in Fig. 3 is a fit of Equation (2) with values given in the caption. As with many experiments, Equation (2) provides a good fit to the data, but there were substantial uncertainties in the fit values given the large number of parameters.

The challenge asked for the viscosity at precise values of pressure and our simulations were at slightly different values. Table 2 gives interpolated values of η_N at the challenge pressures. The second column was obtained from a linear interpolation between neighboring data points from our simulations. The shifts are no larger than the errorbars in Table 1. The final column was obtained from the fit to Equation (2) shown in Fig. 3. The two columns are consistent within the statistical errors of Table 1 and we submitted values from linear interpolation as our official entry.

4. Discussion

The results presented above show that all-atom NEMD simulations can readily reach low enough rates to be in the Newtonian limit for η_N as large as 0.1 Pa·s. With sufficient time, rates of 10^7 s^{-1} and viscosities of 1 Pa·s can be reached. The computational effort grows linearly with viscosity for both nonequilibrium simulations and equilibrium methods based on the fluctuation-dissipation theorem [9]. Thus calculations of viscosities much larger than 1 Pa·s require a different approach. In this paper and Ref. [5], Eyring theory was used to extrapolate high-rate data to the Newtonian limit. For squalane the results were consistent with trends in experimental data over a wide range of pressure and temperature.

For 2,2,4-trimethylhexane the combined approach of direct evaluation and Eyring extrapolation gave values of η_N with numerical uncertainties of about 15% or less. The uncertainties associated with the choice of atomic force field are likely to be much larger. Ewen et al. [21] calculated η_N for n-hexadecane with all-atom and united-atom potentials and found values a factor of 2 lower or higher than experiment. O'Connor [35] found a variation by ±50% in the friction between polyethylene chains calculated with AIREBO-M and other all-atom potentials. Based on these past studies, we expected the systematic error associated with the choice of AIREBO-M to be as large as a factor of 2 in the range of T and P studied here.

The goal of the challenge was to determine how well viscosities can be predicted, so we made no attempt to modify the AIREBO-M force field. It was parameterized based on structural data at high pressures and is expected to be least accurate at ambient pressure and high temperature [24]. More accurate results might be obtained by refitting AIREBO-M to match the known viscosities of molecules similar to the target molecule.

To assess the accuracy of AIREBO-M before the challenge results were announced we compared the results in Table 2 to published experiments. The calculated viscosities have roughly the same magnitude as similar hydrocarbons at lower pressures [36–38]. Johnson and Fawcett [39] measured the viscosity of 2,2,4-trimethylhexane at room temperature and pressure and found a viscosity of 0.648 mPa·s. This is higher than our ambient pressure value by about 40% and at a slightly higher temperature, suggesting that our values might be systematically low by up to 50%. As noted, AIREBO-M was optimized for high pressure. As a check of high pressure accuracy, we used the same model to simulate simple shear of 2,2,4-trimethylpentane, also known as isooctane, at $T = 298$ K, $p = 500$ MPa. The simulations gave a viscosity of 15.3± 0.5 mPa·s, while Dymond [40] reports a measured value that is about 10% smaller, 13.6 mPa·s with an uncertainty of 2%. This is consistent with an increase in the accuracy of AIREBO-M at high pressure.

After the challenge data were announced, we added them to Fig. 3 to facilitate comparison. For all the pressures simulated, the predicted viscosities differ from experiment by less than 40%. This is slightly better than our estimate above of the systematic errors associated with the choice of AIREBO-M. Calculated viscosities are in excellent agreement with experiment at intermediate pressures, with the largest deviations at low and high pressures that we now discuss.

The difference in η_N at ambient conditions is slightly better than expected because the challenge data are lower than previously published values [39]. Some challenge entries were more accurate in this limit because they fit to it or used potentials developed for ambient pressure. Our underestimate of η_N in ambient conditions is consistent with known behavior of AIREBO [41], which is nearly the same as AIREBO-M at ambient pressure. AIREBO gives densities that are too large because it underestimates the attractive cohesive potential. An improved version [41] that uses chemistry dependent van der Waals interactions and includes long-range tail corrections to the pressure [27] provides better densities at ambient pressure but the potential is more complicated and not available through LAMMPS. These van der Waals terms become increasingly irrelevant as pressure increases.

Our predictions capture the viscosity-pressure coefficient and the location of the inflection point in η_N quite accurately but rise slightly too rapidly at the highest pressures. Based on other entries to the challenge, this rise seems to be very sensitive to the potential. Some entries saw no inflection and others found much steeper rises than in our work. For our data the error grows to ∼ 35% as p rises to 1000 MPa. Note that a single simulation at the lowest rate was most critical in determining this largest value and, as noted, this run may not have gone to strains large enough to reach steady state. This typically led to an overestimate of viscosity for squalane [5] and it is possible that additional low rate data would produce values closer

Table 2
Pressures specified in the challenge and corresponding Newtonian viscosities obtained by linear interpolation, η_N^{lin}, and fits to Eq. (2), η_N^{hyb}.

p(MPa)	η_N^{lin}(mPa·s)	η_N^{hyb}(mPa·s)
0.1	0.46 ± 0.05	0.46
25	0.68 ± 0.03	0.69
50	0.96 ± 0.05	0.94
100	1.55 ± 0.04	1.6
150	2.4 ± 0.2	2.4
250	5.5 ± 0.3	5.3
400	15 ± 1	16
500	33 ± 2	33
600	69 ± 3	69
700	146 ± 20	147
800	325 ± 40	320
900	770 ± 60	713
1000	1620 ± 200	1634

to experiment. It would be very interesting to explore still higher pressures with both experiment and simulation to test the hybrid model and predicted divergence of η and to see what is needed to improve interaction potentials.

Acknowledgements

We thank Vikram Jadhao for useful discussions. Funding: This material is based upon work supported by the National Science Foundation under Grant No. DMR-1411144; and the Army Research Laboratory under the MEDE Collaborative Research Alliance, through Grant W911NF-12-2-0022.

References

[1] D. Dowson, G.R. Higginson, Elasto-Hydrodynamic Lubrication, SI Edition, no. 23 in International Series on Materials Science and Technology, Pergamon Press, 1977.
[2] P. Vergne, S. Bair, Classical EHL versus quantitative EHL: a perspective Part I—real viscosity-pressure dependence and the viscosity-pressure coefficient for predicting film thickness, Tribol. Lett. 54 (1) (2014) 1–12, https://doi.org/10.1007/s11249-014-0302-7.
[3] S. Bair, L. Martinie, P. Vergne, Classical EHL versus quantitative EHL: a perspective Part II—Super-Arrhenius piezoviscosity, an essential component of elastohydrodynamic friction missing from classical EHL, Tribol. Lett. 63 (3) (2016) 37, https://doi.org/10.1007/s11249-016-0725-4.
[4] J.P. Ewen, C. Gattinoni, J. Zhang, D.M. Heyes, H.A. Spikes, D. Dini, On the effect of confined fluid molecular structure on nonequilibrium phase behaviour and friction, Phys. Chem. Chem. Phys. 19 (27) (2017) 17883–17894, https://doi.org/10.1039/C7CP01895A.
[5] V. Jadhao, M.O. Robbins, Probing large viscosities in glass-formers with nonequilibrium simulations, Proc. Natl. Acad. Sci. 114 (30) (2017) 7952–7957, https://doi.org/10.1073/pnas.1705978114.
[6] H. Spikes, Z. Jie, History, origins and prediction of elastohydrodynamic friction, Tribol. Lett. 56 (1) (2014) 1–25, https://doi.org/10.1007/s11249-014-0396-y.
[7] S. Bair, P. Vergne, P. Kumar, G. Poll, I. Krupka, M. Hartl, W. Habchi, R. Larsson, Comment on history, origins and prediction of elastohydrodynamic friction by spikes and jie, Tribol. Lett. 58 (1) (2015) 16, https://doi.org/10.1007/s11249-015-0481-x.
[8] H. Spikes, J. Zhang, Reply to the comment by Scott Bair, Philippe Vergne, Punit Kumar, Gerhard Poll, Ivan Krupka, Martin Hartl, Wassim Habchi, Roland Larson on history, origins and prediction of elastohydrodynamic friction by spikes and jie in tribology letters, Tribol. Lett. 58 (1) (2015) 17, https://doi.org/10.1007/s11249-015-0483-8.
[9] M.P. Allen, D.J. Tildesley, Computer Simulation of Liquids, second ed., Oxford University Press, Oxford, United Kingdom, 2017.
[10] M. Mondello, G.S. Grest, Molecular dynamics of linear and branched alkanes, J. Chem. Phys. 103 (16) (1995) 7156–7165, https://doi.org/10.1063/1.470344.
[11] W. Allen, R.L. Rowley, Predicting the viscosity of alkanes using nonequilibrium molecular dynamics: evaluation of intermolecular potential models, J. Chem. Phys. 106 (24) (1997) 10273–10281, https://doi.org/10.1063/1.474052.
[12] C. McCabe, S. Cui, P.T. Cummings, Characterizing the viscositytemperature dependence of lubricants by molecular simulation, Fluid Phase Equilib. 183–184 (2001) 363–370, https://doi.org/10.1016/S0378-3812(01)00448-4.
[13] L.I. Kioupis, E.J. Maginn, Rheology, dynamics, and structure of hydrocarbon blends: a molecular dynamics study of n-hexane/n-hexadecane mixtures, Chem. Eng. J. 74 (1–2) (1999) 129–146, https://doi.org/10.1016/S1385-8947(99)00053-4.
[14] H. Tamura, M. Yoshida, K. Kusakabe, Chung, R. Miura, M. Kubo, K. Teraishi, A. Chatterjee, A. Miyamoto, Molecular dynamics simulation of friction of hydrocarbon thin films, Langmuir 15 (22) (1999) 7816–7821, https://doi.org/10.1021/la9805084.
[15] H. Yamano, K. Shiota, R. Miura, M. Katagiri, M. Kubo, A. Stirling, E. Broclawik, A. Miyamoto, T. Tsubouchi, Molecular dynamics simulation of traction fluid molecules under EHL condition, Thin Solid Films 281–282 (1996) 598–601, https://doi.org/10.1016/0040-6090(96)08697-X.
[16] L.I. Kioupis, E.J. Maginn, Impact of molecular architecture on the high-pressure rheology of hydrocarbon fluids, J. Phys. Chem. B 104 (32) (2000) 7774–7783, https://doi.org/10.1021/jp000966x.
[17] S. Bair, C. McCabe, P.T. Cummings, Comparison of nonequilibrium molecular dynamics with experimental measurements in the nonlinear shear-thinning regime, Phys. Rev. Lett. 88 (5) (2002) 058302, https://doi.org/10.1103/PhysRevLett.88.058302.
[18] C. McCabe, C.W. Manke, P.T. Cummings, Predicting the Newtonian viscosity of complex fluids from high strain rate molecular simulations, J. Chem. Phys. 116 (8) (2002) 3339–3342, https://doi.org/10.1063/1.1446045.
[19] P.A. Gordon, Development of intermolecular potentials for predicting transport properties of hydrocarbons, J. Chem. Phys. 125 (1) (2006) 014504, https://doi.org/10.1063/1.2208359.
[20] H. Eyring, Viscosity, plasticity, and diffusion as examples of absolute reaction rates, J. Chem. Phys. 4 (4) (1936) 283–291, https://doi.org/10.1063/1.1749836.
[21] J. Ewen, C. Gattinoni, F. Thakkar, N. Morgan, H. Spikes, D. Dini, A comparison of classical force-fields for molecular dynamics simulations of lubricants, Materials 9 (8) (2016) 651, https://doi.org/10.3390/ma9080651.
[22] S.J. Stuart, A.B. Tutein, J.A. Harrison, A reactive potential for hydrocarbons with intermolecular interactions, J. Chem. Phys. 112 (14) (2000) 6472–6486, https://doi.org/10.1063/1.481208.
[23] D.W. Brenner, O.A. Shenderova, J.A. Harrison, S.J. Stuart, B. Ni, S.B. Sinnott, A second-generation reactive empirical bond order (REBO) potential energy expression for hydrocarbons, J. Phys. Condens. Matter 14 (4) (2002) 783–802, https://doi.org/10.1088/0953-8984/14/4/312.
[24] T.C. O'Connor, J. Andzelm, M.O. Robbins, AIREBO-M: a reactive model for hydrocarbons at extreme pressures, J. Chem. Phys. 142 (2) (2015), 024903, https://doi.org/10.1063/1.4905549.
[25] S. Plimpton, Fast parallel algorithms for short-range molecular dynamics, J. Comput. Phys. 117 (1) (1995) 1–19, https://doi.org/10.1006/jcph.1995.1039.
[26] D.J. Evans, G.P. Morriss, Nonlinear-response theory for steady planar Couette flow, Phys. Rev. A 30 (3) (1984) 1528–1530, https://doi.org/10.1103/PhysRevA.30.1528.
[27] D. Frenkel, B. Smit, Understanding Molecular Simulation: from Algorithms to Applications, second ed., no. 1 in Computational Science Series, Academic Press, San Diego, 2002.
[28] V. Jadhao, M.O. Robbins, Rheological Properties of Liquids under Conditions of Elastohydrodynamic Lubrication. arXiv:1903.03996 [cond-mat].
[29] M. Paluch, Z. Dendzik, S.J. Rzoska, Scaling of high-pressure viscosity data in low-molecular-weight glass-forming liquids, Phys. Rev. B 60 (5) (1999) 2979–2982, https://doi.org/10.1103/PhysRevB.60.2979.
[30] H. Vogel, Das temperaturabhaengigkeitsgesetz der viskositaet von fluessigkeiten, Phys. Z. 22 (1921) 645.
[31] G. Tammann, W. Hesse, Die Abhngigkeit der Viscositt von der Temperatur bie unterkhlten Flssigkeiten, Z. Anorg. Allg. Chem. 156 (1) (1926) 245–257, https://doi.org/10.1002/zaac.19261560121.
[32] G.S. Fulcher, Analysis of recent measurements of the viscosity of glasses, J. Am. Ceram. Soc. 8 (6) (1925) 339–355, https://doi.org/10.1111/j.1151-2916.1925.tb16731.x.
[33] E. McEwen, The effect of variation of viscosity with pressure on the load-carrying capacity of the oil film between gear teeth, J. Inst. Pet. 38 (344–345) (1952) 646–672.
[34] S. Bair, Choosing pressure-viscosity relations, High. Temp. - High. Press. 44 (6) (2015) 415–428.
[35] T.C. O'Connor, The Nonlinear Mechanics and Rheology of Oriented Polymers, Ph.D. thesis, Johns Hopkins University, 2018.
[36] J.H. Dymond, K.J. Young, J.D. Isdale, Transport properties of nonelectrolyte liquid mixtures—II. Viscosity coefficients for the n-hexane + n-hexadecane system at temperatures from 25 to 100C at pressures up to the freezing pressure or 500 MPa, Int. J. Thermophys. 1 (4) (1980) 345–373, https://doi.org/10.1007/BF00516563.
[37] J.H. Dymond, J. Robertson, J.D. Isdale, Transport properties of nonelectrolyte liquid mixtures—III. Viscosity coefficients for n-octane, n-dodecane, and equimolar mixtures of n-octane + n-dodecane and n-hexane + n-dodecane from 25 to 100C at pressures up to the freezing pressure or 500 MPa, Int. J. Thermophys. 2 (2) (1981) 133–154, https://doi.org/10.1007/BF00503937.
[38] C.M.B.P. Oliveira, W.A. Wakeham, The viscosity of five liquid hydrocarbons at pressures up to 250 MPa, Int. J. Thermophys. 13 (5) (1992) 773–790, https://doi.org/10.1007/BF00503906.
[39] G.C. Johnson, F.S. Fawcett, Inter-polymerization of isobutene and 2-Methyl-2-butene using an alumina-silica catalyst. Composition of the hydrogenated nonenes, J. Am. Chem. Soc. 68 (8) (1946) 1416–1419, https://doi.org/10.1021/ja01212a005.
[40] J.H. Dymond, N.F. Glen, J.D. Isdale, Transport properties of nonelectrolyte liquid mixtures—VII. Viscosity coefficients for isooctane and for equimolar mixtures of isooctane + n-octane and isooctane + n-dodecane from 25 to 100C at pressures up to 500 MPa or to the freezing pressure, Int. J. Thermophys. 6 (3) (1985) 233–250, https://doi.org/10.1007/BF00522146.
[41] A. Liu, S.J. Stuart, Empirical bond-order potential for hydrocarbons: adaptive treatment of van der Waals interactions: empirical bond-order potential for hydrocarbons, J. Comput. Chem. 29 (4) (2008) 601–611, https://doi.org/10.1002/jcc.20817.